

RESEARCH

Open Access



# Increased distribution of carbon metabolic flux during de novo cytidine biosynthesis via attenuation of the acetic acid metabolism pathway in *Escherichia coli*

Tong Ye<sup>1,3</sup>, Wei Ding<sup>2,3</sup>, Zhengxu An<sup>2</sup>, Haojie Zhang<sup>2,3</sup>, Xiaobo Wei<sup>2,3</sup>, Junnan Xu<sup>2,3</sup>, Huiyan Liu<sup>2,3\*</sup> and Haitian Fang<sup>1,2,3\*</sup>

## Abstract

Acetic acid, a by-product of cytidine synthesis, competes for carbon flux from central metabolism, which may be directed either to the tricarboxylic acid (TCA) cycle for cytidine synthesis or to overflow metabolites, such as acetic acid. In *Escherichia coli*, the acetic acid synthesis pathway, regulated by the *poxB* and *pta* genes, facilitates carbon consumption during cytidine production. To mitigate carbon source loss, the CRISPR-Cas9 gene-editing technique was employed to knock out the *poxB* and *pta* genes in *E. coli*, generating the engineered strains K12 $\Delta$ *poxB* and K12 $\Delta$ *poxB* $\Delta$ *pta*. After 39 h of fermentation in 500 mL shake flasks, the cytidine yields of strains K12 $\Delta$ *poxB* and K12 $\Delta$ *poxB* $\Delta$ *pta* were  $1.91 \pm 0.04$  g/L and  $18.28 \pm 0.22$  g/L, respectively. Disruption of the *poxB* and *pta* genes resulted in reduced acetic acid production and glucose consumption. Transcriptomic and metabolomic analyses revealed that impairing the acetic acid metabolic pathway in *E. coli* effectively redirected carbon flux toward cytidine biosynthesis, yielding a 5.26-fold reduction in acetate metabolism and an 11.56-fold increase in cytidine production. These findings provide novel insights into the influence of the acetate metabolic pathway on cytidine biosynthesis in *E. coli*.

**Keywords** Acetate metabolism, Carbon metabolic flux, Cytidine, *Escherichia coli*

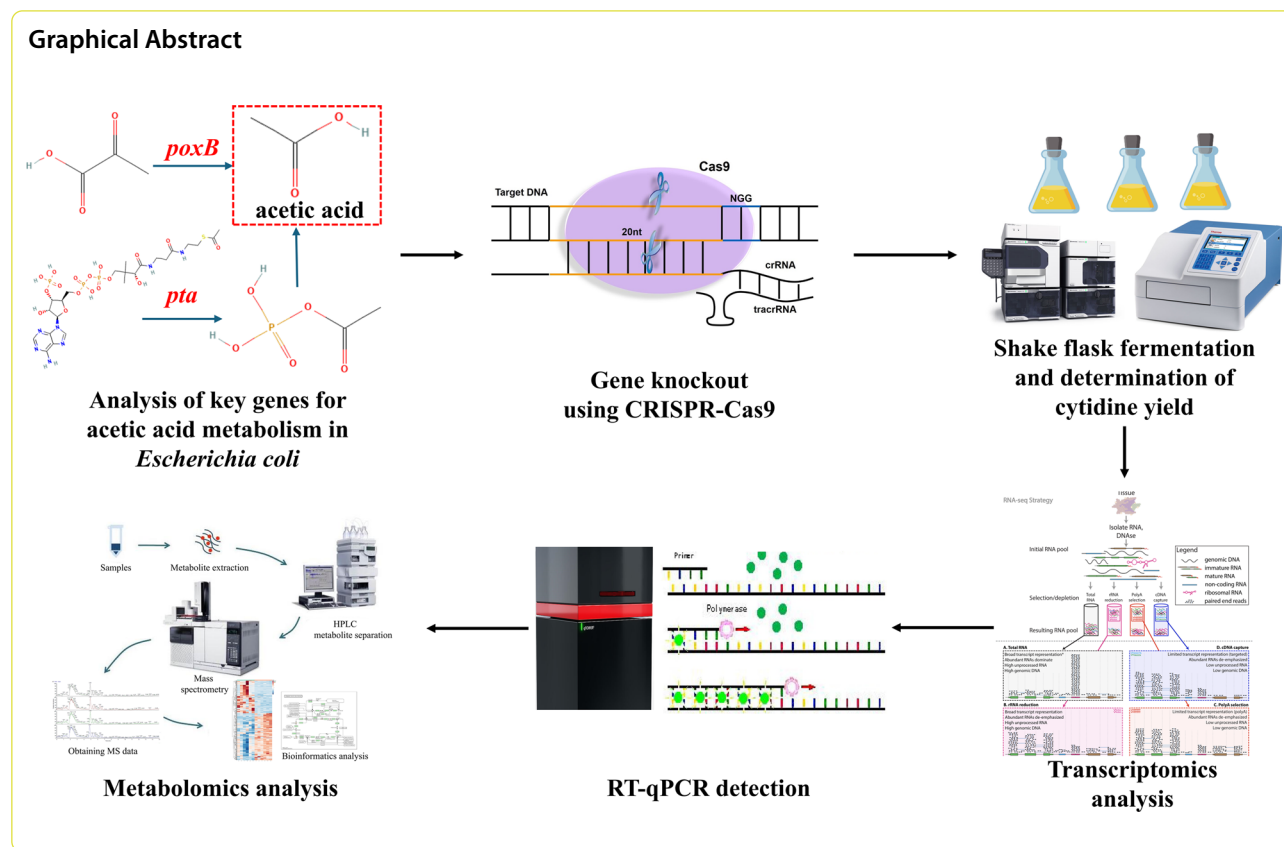
\*Correspondence:

Huiyan Liu  
liuhy@nxu.edu.cn  
Haitian Fang  
fanght@nxu.edu.cn

Full list of author information is available at the end of the article



© The Author(s) 2025. **Open Access** This article is licensed under a Creative Commons Attribution-NonCommercial-NoDerivatives 4.0 International License, which permits any non-commercial use, sharing, distribution and reproduction in any medium or format, as long as you give appropriate credit to the original author(s) and the source, provide a link to the Creative Commons licence, and indicate if you modified the licensed material. You do not have permission under this licence to share adapted material derived from this article or parts of it. The images or other third party material in this article are included in the article's Creative Commons licence, unless indicated otherwise in a credit line to the material. If material is not included in the article's Creative Commons licence and your intended use is not permitted by statutory regulation or exceeds the permitted use, you will need to obtain permission directly from the copyright holder. To view a copy of this licence, visit <http://creativecommons.org/licenses/by-nc-nd/4.0/>.



## Introduction

The acetic acid metabolic pathway in *Escherichia coli* plays a critical role in the organism's acid production. Due to the high glucose intake, *E. coli* cells often fail to completely oxidize glucose, leading to the utilization of acetic acid as an alternative form of energy storage [1–3]. However, acetic acid is highly cytotoxic, with the potential to disrupt the cell membrane's permeability [4–6]. Additionally, acetic acid can lower the pH of the surrounding environment, thereby enhancing the uptake of bacterial carbon sources. This increase in acetic acid metabolism can consequently reduce the yield of target products [6, 7]. The acetic acid metabolic pathway in *E. coli* is primarily governed by two enzyme systems: POXB (pyruvate oxidase) and PTA (phosphotransacetylase), both of which are essential for acetic acid biosynthesis [8, 9]. Upon disruption of this metabolic pathway, an increase in the levels of target products has been observed. Specifically, targeted gene knockouts of *ackA-pta*, *poxB*, *ldhA*, *adhE*, *ptsG*, *aceBAK*, *glcB*, and *sdhAB* resulted in a glucose-to-succinate conversion rate of 93% [10]. Similarly, knockdown of the *yqhD*, *poxB*, and *pta-ackA* genes led to a significant increase in 3-hydroxypropionic acid concentration, rising from 440 to 556 mM [11]. However, there remains a notable gap in

research regarding the modulation of the *E. coli* acetate metabolic pathway to enhance cytidine production.

Cytidine, a pyrimidine nucleoside present in all living organisms, plays a pivotal role in RNA synthesis and is involved in numerous physiological and biochemical processes [12]. The pharmaceutical industry requires substantial quantities of cytidine for the production of antitumor and anticancer drugs, such as cytarabine and cyclocytidine [13]. Cytidine can be synthesized through two primary methods: enzymatic hydrolysis of ribonucleic acid (RNA) and microbial fermentation. However, the use of RNA for enzymatic hydrolysis in cytidine synthesis is constrained by challenges in reaction control, by-product formation, and high substrate demands [14]. As a result, microbial fermentation has become the dominant method for cytidine production, owing to its scalability and efficiency. *E. coli* is an ideal host for genetic modification due to its favourable cellular properties and ease of cultivation [15]. For instance, Dai et al. enhanced pyrimidine nucleoside biosynthesis through modular reconstruction of the pyrimidine pathway in *E. coli*, achieving a final cytidine yield of 8.1 g/L [16]. Similarly, Yang et al. inhibited the UMP pathway for cytidine catabolism and increased precursor availability, resulting in a genetically engineered *E.*

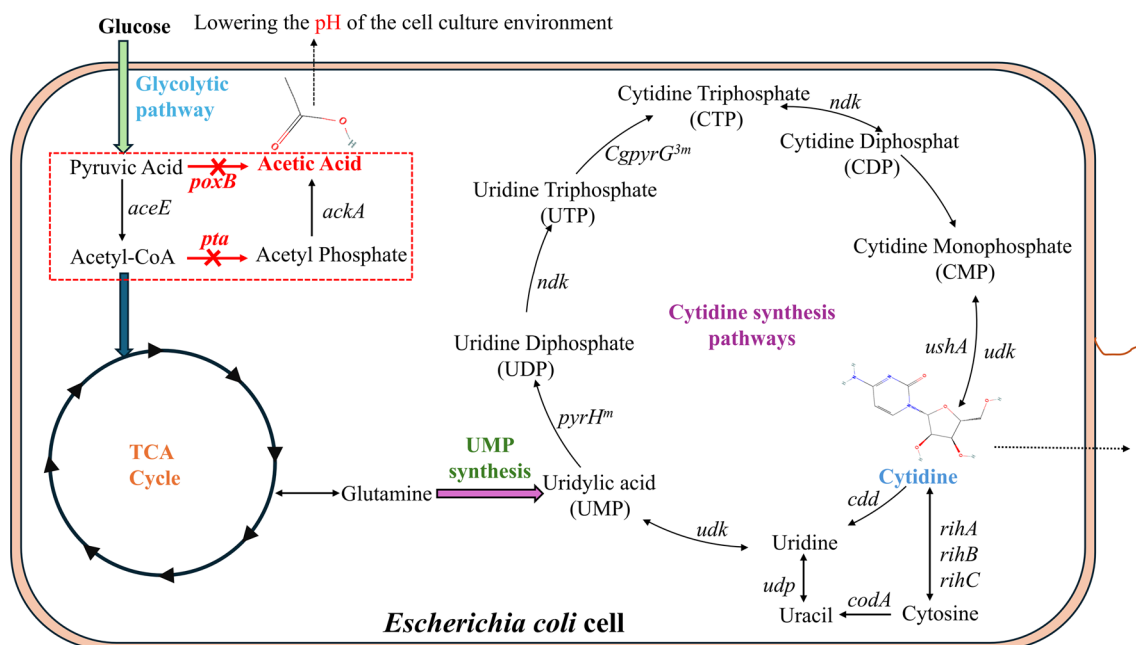


**Fig. 1** Main biological pathways for cytidine synthesis in *E. coli*. Precursor synthesis is divided into the pentose phosphate pathway, glycolysis, and the TCA cycle, which provide the necessary precursors for cytidine synthesis. UMP synthesis primarily involves the production of uridylic acid (UMP). The cytidine synthesis pathway utilizes UMP as a precursor to synthesize cytidine. The boxed section in the figure highlights the gene editing aspect of this study, with the red X indicating the site of knockout [17]

*coli* strain that produced 7.84 g/L cytidine after 40 h of fermentation in a 5 L fermenter [17].

As illustrated in Fig. 1 and Fig. S1, the biosynthesis of cytidine in *E. coli* involves a complex network of three distinct pathways: the precursor synthesis pathway, which includes glycolysis and the tricarboxylic acid (TCA) cycle; the uridylic acid (UMP) synthesis pathway; and the cytidine synthesis cycle [17, 18]. While prior studies have focused on modifying the upstream and downstream pathways of cytidine biosynthesis, there has been limited investigation into the precursor synthesis and acetic acid metabolic pathways in *E. coli*.

To mitigate the impact of the acetic acid metabolic pathway in *E. coli*, which adversely affects the cellular environment and depletes organic carbon, thereby reducing cytidine synthesis, this study employed a sequential knockout strategy targeting the key genes *poxB* and *pta*. This approach resulted in the construction of two genetically engineered strains, *E. coli* K12 $\Delta$ *poxB* and *E. coli* K12 $\Delta$ *poxB* $\Delta$ *pta*. Using transcriptomic and metabolomic analyses, key differences in gene expression and metabolic profiles were examined before and after gene knockout, enabling a detailed investigation of the changes in carbon flux. These analyses provided insights into the underlying mechanisms driving the observed alterations in cytidine production following the disruption of key acetic acid metabolic pathways.

The experimental framework is depicted in Fig. 2. The results of this study enhance our understanding of how the acetic acid metabolic pathway influences cytidine biosynthesis in *E. coli* and offer a theoretical foundation for optimizing the efficient production of cytidine in microbial systems.

## Materials and methods

### Strains and culture conditions

The strains and plasmids employed or generated in this study are summarized in Table S1 (Supplementary Material 2, Table S1). The growth conditions for these strains involved culturing them in 50 mL shake flasks containing 25 mL of LB medium (Sangon Biotech Shanghai Co., Ltd.) for 39 h. Cytidine fermentation was performed in an LB medium supplemented with glucose. The fermentation setup included 100 mL of medium in a 500 mL shake flask, composed of 90 mL of LB medium and 10 mL of glucose at a concentration of 500 g/L, yielding a final volume of 100 mL. Additional glucose (10 mL at 500 g/L) was introduced at the 8th and 24th h of the fermentation. The fermentation process was conducted at a constant temperature of 37 °C over a period of 39 h, with shaking at 200 rpm. During this process, pH, residual sugar, and cytidine content were monitored. To ensure reliability, samples were collected

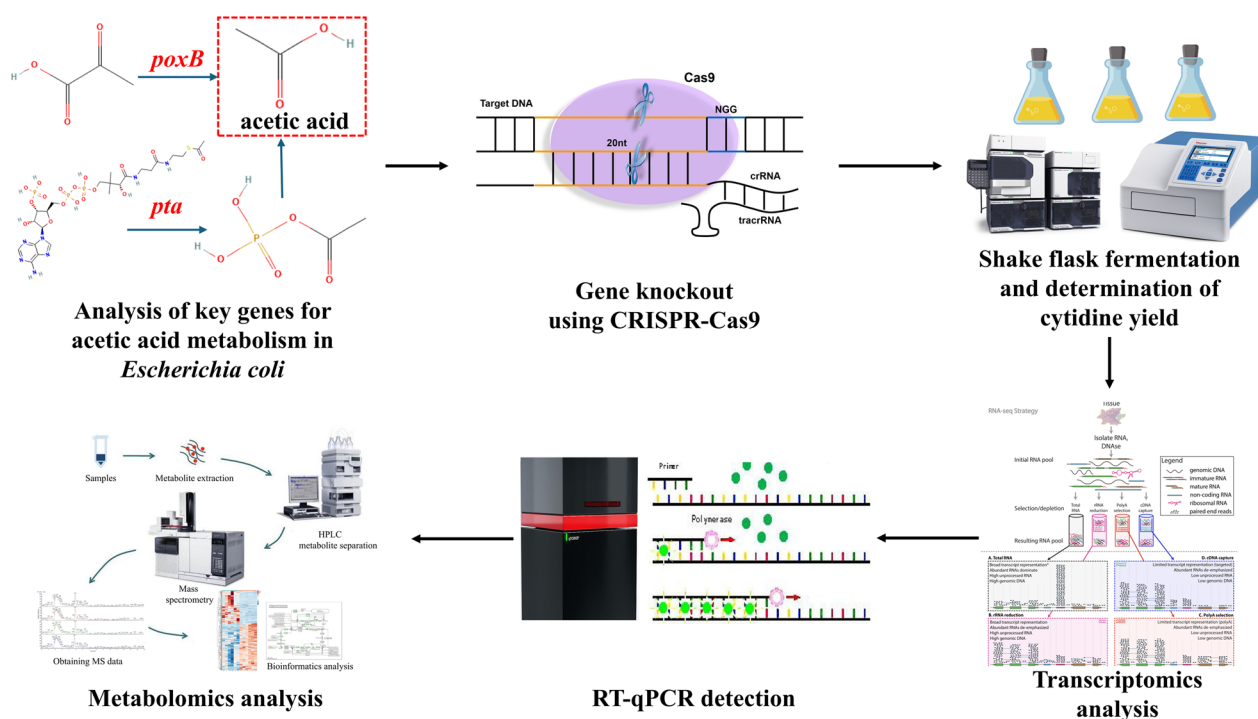


**Fig. 2** Schematic of the research methodology: this figure outlines the comprehensive analysis conducted to examine the changes in cytidine production and the underlying mechanisms following the knockout of key genes involved in acetic acid metabolism. The process includes the identification of critical genes for acetic acid metabolism, gene knockout, cytidine and other product quantification, transcriptomic analysis, RT-qPCR validation, and metabolomic profiling

every 4 h up to 24 h, and every 3 h from 24 to 39 h, with 2 mL samples taken at each time point.

### Knockout of the *poxB* and *pta* genes

Gene knockout was performed following the protocol described by Liu et al. [19], utilizing the CRISPR-Cas9 gene editing system to knock out the *poxB* (NC\_000913.3:c911049-909331) and *pta* (NC\_000913.3:2414747-2416891) genes in *E. coli* K12MG1655 (NCBI Taxonomy ID 511145, RefSeq: GCF\_000005845.2, NC\_000913.3). The sequences and functions of the primers used are provided in Table S2 (Supplementary Material 3, Table S2). PCR conditions are outlined in Supplementary Material 4, while the enzyme digestion reaction conditions are detailed in Supplementary Material 5.

### Growth curve, cytidine yield, residual sugar, and pH measurements

The growth curve of *E. coli* was monitored by measuring the OD<sub>600</sub> using a BioTek Epoch 2 microplate spectrophotometer (Agilent) and 96-well cell culture plates (Servicebio, CCP-96H plates, PS lids, bore diameter 6.45 mm). Each well was filled with 198  $\mu$ L of glucose-enriched LB medium and 2  $\mu$ L of an *E.*

*coli* bacterial mixture, which was incubated at 37 °C with shaking at 220 rpm for 48 h. Evaporation was continuously monitored, and OD<sub>600</sub> readings were recorded every 15 min. pH measurements were taken during fermentation using a Rex laboratory pH meter (Shanghai Yidian Scientific Instrument Co., Ltd.). Following fermentation, the culture broth was filtered through a needle filter, and cytidine yield was quantified by high-performance liquid chromatography (HPLC; LC-16, Shimadzu) with a UV detector, using an Agilent C<sub>18</sub> reversed-phase column (4.6  $\times$  150 mm). The mobile phase consisted of water:acetonitrile in a 96:4 ratio at a flow rate of 1 mL/min, with isocratic elution at a column temperature of 30 °C and detection at 270 nm [19]. Residual sugar content in the culture broth was measured with an SBA-40E Biosensor Analyzer (Jinan Yanhe Biotechnology Co., Ltd.) according to the manufacturer's instructions. All experiments were performed under identical conditions to ensure data consistency.

### Transcriptomic assays

Total RNA from *E. coli* K12, *E. coli* K12 $\Delta$ *poxB*, and *E. coli* K12 $\Delta$ *poxB* $\Delta$ *pta* was extracted at the 39-h time point of fermentation using the Omega Biotek Bacterial RNA Kit (R6950), following the procedure outlined

in the manufacturer's instructions. The RNA samples were subsequently sent to Shanghai Sangon Biotech for quality control and transcriptomic analysis. After RNA purification and verification, sequencing libraries were prepared, and high-throughput sequencing was performed on the NovaSeq platform. Data quality was assessed, and the sequences were aligned to the reference genome using HISAT2 software. Gene expression levels and differential expression analysis were conducted using StringTie and DESeq2. Differentially expressed genes (DEGs) were identified with a  $q$  value  $\leq 0.05$  and a  $|\text{fold change}| \geq 2$ . Comparisons were made between *E. coli* K12 and the knockout strains (*E. coli* K12 $\Delta$ *poxB* vs *E. coli* K12, referred to as B vs K; *E. coli* K12 $\Delta$ *poxB* $\Delta$ *pta* vs *E. coli* K12, referred to as A vs K; and *E. coli* K12 $\Delta$ *poxB* $\Delta$ *pta* vs *E. coli* K12 $\Delta$ *poxB*, referred to as A vs B). Gene Ontology (GO) and Kyoto Encyclopedia of Genes and Genomes (KEGG) enrichment analyses were performed to explore the biological significance of DEGs. Detailed transcriptomic analysis methods are provided in Supplementary Material 6.

#### Real-time quantitative PCR (RT-qPCR)

Total RNA was extracted from *E. coli* strains K12, K12 $\Delta$ *poxB*, and K12 $\Delta$ *poxB* $\Delta$ *pta* after 39 h of fermentation using the Bacterial RNA Kit (R6950). The RNA purity was assessed using a NanoOne Microspectrophotometer (Hangzhou Yooning Instrument Co., Ltd.). Reverse transcription was performed using PrimeScript<sup>TM</sup> RT Master Mix (Perfect Real Time) (TaKaRa). RT-qPCR was conducted with TB Green<sup>®</sup> Premix Ex Taq<sup>TM</sup> II (Tli RNaseH Plus) (TaKaRa) and the respective gene-specific primers (sequences and functions provided in Supplementary Material 7, Table S3). The relative expression of genes was normalized to 16S rRNA as the internal control, and the expression levels were calculated using the  $-\log_2(\Delta\Delta Ct)$  method. Detailed RT-qPCR procedures can be found in Supplementary Material 8.

#### Metabolomics assays

A quality control (QC) sample, comprising a mixture of portions from each analytical sample, was prepared to ensure system stability and result reliability. Metabolite analysis of fermentation broths from various samples collected at the 39-h time point was conducted using an ultrahigh-performance liquid chromatography-tandem mass spectrometry (UHPLC-MS/MS) system. The samples were subjected to liquid chromatography on an ACQUITY UPLC<sup>®</sup> HSS T3 column, followed by mass spectrometry data acquisition through electrospray ionization (ESI) in both positive and negative modes (Supplementary Material 9). Data preprocessing and peak alignment were performed using MS-DIAL software to

ensure accurate peak identification and quantification. Multivariate statistical analyses were conducted using R software, with models developed through principal component analysis (PCA), orthogonal partial least squares discriminant analysis (PLS-DA), and partial least squares discriminant analysis (OPLS-DA). Alignment tests were performed to assess potential model overfitting. Notably, metabolites showing significant differences between groups were identified based on variable importance projection (VIP) values and two-tailed t-tests. Further, KEGG enrichment analyses were performed to uncover relevant biological pathways.

#### Statistical analysis

Statistical analysis was conducted using SPSS 26.0 (IBM, Chicago, USA) for analysis of variance (ANOVA) and least significant difference (LSD) Fisher's test, with statistical significance set at  $P < 0.05$ . Data visualization was performed using Origin 2024 (OriginLab, Northampton, MA). All experiments were repeated three times, with metabolomics experiments repeated six times. The results are expressed as means  $\pm$  standard deviations ( $\bar{X} + SD$ ).

## Results and discussion

### Effects of the knockout of a key gene for acetic acid metabolism on cytidine production

To modify the acetic acid metabolic pathway in *E. coli* for enhanced cytidine production, the *poxB* and *pta* genes of *E. coli* K12 were knocked out using the CRISPR-Cas9 gene editing system, resulting in two new strains: *E. coli* K12 $\Delta$ *poxB* and *E. coli* K12 $\Delta$ *poxB* $\Delta$ *pta*. As shown in Fig. S2, the successful knockout of the *poxB* and *pta* genes was confirmed through sequencing, with lanes 2, 4, and 5 exhibiting bands near 250 bp, indicating the knockout of the target genes in a sequential manner (see Supplementary Materials 10–13, Sequences S1–S4 for sequencing results). The growth curves, presented in Fig. 3A, visually demonstrate the changes in bacterial biomass. The knockout of the *poxB* gene had minimal impact on bacterial growth. However, the knockout of the *pta* gene resulted in a significant delay in the logarithmic growth phase. After 10 h, the OD<sub>600</sub> value of K12 $\Delta$ *poxB* $\Delta$ *pta* was notably higher than that of both the K12 and K12 $\Delta$ *poxB* strains, indicating that the *pta* knockout promotes greater biomass accumulation in *E. coli* and delays the onset of the logarithmic growth phase. These results are consistent with those of Castaño-Cerezo [9], supporting the idea that the disruption of the *pta* gene affects the growth dynamics and biomass accumulation in *E. coli*. The change in pH provides an indicator of the acidity and alkalinity shifts within the culture system, as shown in Fig. 3B, which illustrates the

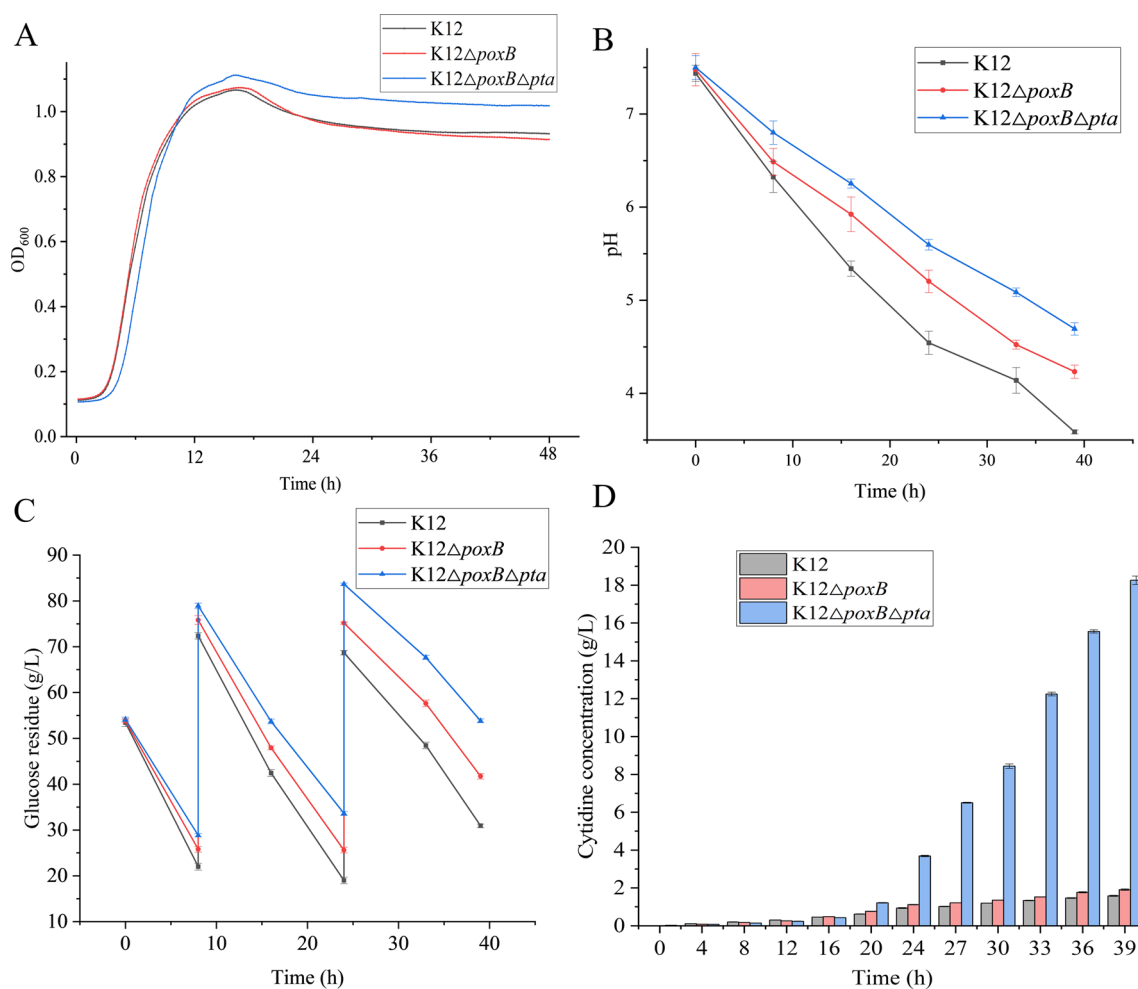


**Fig. 3** Shake flask fermentation results of genetically engineered *E. coli* strains. **A** Growth curve analysis; **B** pH changes in the fermentation system; **C** residual sugar content determination in the fermentation system; **D** cytidine concentration measurement in the fermentation system

pH variations during cytidine fermentation of the *E. coli* K12, K12ΔpoxB, and K12ΔpoxBΔpta strains. The pH of the original *E. coli* K12 strain decreased significantly during the fermentation process. In contrast, the K12ΔpoxB strain exhibited a slower pH decline, while the pH of the K12ΔpoxBΔpta strain decreased the most gradually. This gradual decrease in pH following the knockout of the acetate metabolism genes suggests that the acetate metabolism pathway plays a significant role in acid production during *E. coli* fermentation. As the acetate metabolism pathway was either weakened or knocked out, the pH of the bacterial culture system became more stable, which is indicative of enhanced cellular survival. These findings align with the results of Gecse et al. [20], providing further insight into the increased cell biomass observed in the K12ΔpoxBΔpta strain. Sugar consumption serves as an indicator of the cell's ability to intake and metabolize glucose. Enhanced growth or conversion activity under equivalent sugar

consumption suggests greater cellular activity. Figure 3C illustrates the residual glucose in the *E. coli* culture system, revealing a notable increase in residual sugar after the gradual knockout of the *poxB* and *pta* genes in the K12 strain. This suggests that the downregulation of acetic acid metabolism genes reduces sugar consumption, conserving carbon sources for the bacterium and minimizing byproduct formation [21]. These results indicate that the knockout of key acetic acid metabolism genes, such as *poxB* and *pta*, enhances the biosynthetic activity of *E. coli*, consistent with the findings of Zhang et al. [22].

The primary objective of genetic modification in this study was to enhance cytidine yield, as illustrated in Fig. 3D, which presents the cytidine production of both the original and engineered *E. coli* strains during 39 h of shake flask fermentation. At the 39-h mark, the cytidine yield for the original *E. coli* K12 strain was  $1.58 \pm 0.03$  g/L. In contrast, the engineered strain K12ΔpoxB produced

1.91 ± 0.04 g/L of cytidine, while the K12Δ*poxB*Δ*pta* strain achieved a significantly higher yield of 18.28 ± 0.22 g/L. This yield surpasses the 2.1 g/L cytidine production reported by Liu et al. [19] in shake flask fermentation and the 15.7 g/L yield achieved by Zhang et al. [23] in a 5 L fermenter. The cytidine yield observed in this study represents the highest level produced by *E. coli* in shake flask fermentation, suggesting that the engineered strain is well-positioned to support industrial-scale cytidine production.

These results demonstrate that inhibiting the acetate metabolic pathway is an effective strategy for enhancing cytidine production. However, the knockout of the *poxB* gene alone did not result in a significant increase in cytidine yield, implying that the knockout of a single gene in the acetic acid metabolism pathway may trigger compensatory pathways. These alternative pathways could potentially redistribute carbon fluxes and energy, leading to inefficiencies and limiting the increase in cytidine production. This hypothesis is further supported by the substantial rise in cytidine yield observed in the K12Δ*poxB*Δ*pta* strain. The analysis of Fig. 3D reveals that cytidine production in shake flask fermentation occurs in two distinct phases: the cell expansion phase and the cytidine fermentation phase. During the cytidine fermentation phase, the bacterial biomass remained relatively constant, a phenomenon primarily driven by the interplay of environmental constraints and the inherent growth characteristics of *E. coli*. Notably, during the logarithmic growth phase (log phase), bacterial metabolism is largely focused on rapid cell division and growth rather than the accumulation of intracellular products, which explains the stable biomass observed during this phase. In addition, environmental factors such as pH and nutrient availability play a critical role in influencing bacterial growth, though the stabilization of biomass in the cytidine production phase is likely more closely linked to the metabolic demands of bacterial growth rather than to pH changes or glucose addition timing [24]. The delayed cytidine production phase, which extended before 16 h of fermentation, showed that the yield of cytidine from the engineered strains was marginally lower than that of the parent strain K12. This observation aligns with the growth curve results (Fig. 3A), where bacterial energy was predominantly dedicated to growth and reproduction, leaving insufficient metabolic fluxes for substantial cytidine accumulation [25]. However, after 24 h of fermentation, a significant increase in cytidine production was observed, signalling the onset of a rapid accumulation phase. During this period, *E. coli* biomass remained relatively stable, with organic carbon predominantly allocated to maintain cellular metabolism and support

cytidine biosynthesis. This suggests that the knockout of key genes involved in acetate metabolism promotes the reallocation of carbon flux towards cytidine biosynthesis, while simultaneously reducing acetate production. As a result, *E. coli* demonstrates an improved ability to convert glucose into cytidine, reinforcing the findings from the preceding pH study (Fig. 3B). Although the knockout of the *poxB* and *pta* genes in *E. coli* resulted in a significant increase in cytidine production, the precise mechanisms underlying this enhancement remain poorly understood. Further investigation is required to delineate the impact of these key acetic acid metabolism gene knockouts on both the carbon metabolism pathway and the cytidine biosynthesis pathway.

#### **Transcriptomic analysis provides insights into the enhanced cytidine accumulation mediated by *poxB* and *pta* knockout**

To elucidate the molecular mechanisms underlying the knockout of key genes involved in acetic acid metabolism in *E. coli* and the subsequent increase in cytidine production, transcriptomic analysis was conducted to investigate the metabolic regulatory dynamics that contribute to enhanced cytidine synthesis at the conclusion of fermentation. The sequencing data were analyzed for correlations between transcript expression profiles (see Supplementary Material 15–17, Table S4, Fig. S3, S4, for quality control results). As shown in Fig. S5 and Fig. S9A, S9B, strong intragroup correlations and significant intergroup variation were observed, indicating distinct expression patterns among the K12, K12Δ*poxB*, and K12Δ*poxB*Δ*pta* strains. These results suggest that the knockout of the *poxB* gene substantially affects *E. coli* metabolism, potentially by activating certain acetic acid metabolic pathways that enable the cells to sustain and continue acid production even after the loss of *poxB*. Additionally, this could involve a redistribution and reprogramming of carbon metabolic fluxes, consistent with the findings of Li et al. [26]. However, the number of DEGs in K12Δ*poxB*Δ*pta* was relatively low compared to the K12 strain. This may be attributed to the complete modification of the acetic acid metabolic pathway, which has resulted in a relative equilibrium in the internal metabolic capacity of the bacteria. After the double knockout, the transcriptional profile of K12Δ*poxB*Δ*pta* was restored to a level comparable to the wild-type strain, indicating that the deletion of the *poxB* and *pta* genes, while central to acetic acid metabolism, did not cause a persistent disruption in the transcriptional network. Instead, a compensatory mechanism was likely activated through the modulation of other metabolic pathways. Comparative transcriptomic analyses of K12Δ*poxB*Δ*pta* and K12 revealed only minor transcriptional

differences, suggesting that *E. coli* exhibits considerable metabolic plasticity and flexibility in its transcriptional regulatory network. Even in the absence of key genes, the bacterium was able to adjust gene expression in response to environmental changes, ensuring survival and maintaining function. This small transcriptional discrepancy may be due to the bacterium's compensation for the loss of acetate metabolism through alternative metabolic routes, thereby preserving the stability and coordination of the broader metabolic network [27–30]. As a result, more carbon is directed toward cell growth and product synthesis, in line with the growth curve results (Fig. 3A) discussed earlier. Additionally, the variability in transcription between  $K12\Delta poxB\Delta pta$  and  $K12\Delta poxB$  (Fig. S9B) further supports this observation.

To elucidate the differential genes and associated metabolic pathways, a KEGG enrichment analysis was conducted to further investigate the pathways and genes linked to cytidine synthesis, as illustrated in Fig. S9 C and Figs. S6–S12, which present the GO and KEGG functional enrichment maps for the comparative groups. In comparison to the K12 strain, the upregulated DEGs in  $K12\Delta poxB$  were primarily enriched in pathways such as nucleotide metabolism, energy metabolism, and carbon metabolism. Conversely, the downregulated DEGs were predominantly enriched in signal transduction pathways, suggesting that the knockout of *poxB* induces a redistribution of carbon metabolic fluxes within *E. coli* [31]. This redistribution likely results in an enhancement of nucleotide and energy metabolism, with a shift in intracellular carbon fluxes towards cytidine synthesis due to the downregulation of genes involved in acetate metabolism. In  $K12\Delta poxB\Delta pta$ , the upregulated DEGs were chiefly linked to pathways involved in energy metabolism, carbon metabolism, and nucleotide metabolism. The downregulated DEGs were predominantly enriched in pathways related to carbon metabolism, lipid metabolism, and amino acid metabolism. The double knockout of the *poxB* and *pta* genes led to further metabolic reorganization in *E. coli*, marked by a significant upregulation of pathways supporting cytidine synthesis, including energy and nucleoside metabolism. Concurrently, pathways related to cytidine catabolism, such as amino acid synthesis and glycolysis, were notably downregulated. These results suggest that the deletion of *poxB* and *pta* may enhance cytidine production by modulating the reduction in byproduct formation and promoting carbon flux toward cytidine biosynthesis. Compared to  $K12\Delta poxB$ , the genes upregulated in  $K12\Delta poxB\Delta pta$  were predominantly associated with nucleotide biosynthesis and carbon metabolism, while downregulated genes were mainly involved in carbon metabolism, energy metabolism, and

amino acid metabolism. Comparative transcriptomic analysis between wild-type and knockout strains revealed significant changes in gene expression, excluding *pta* and *poxB*, which may play pivotal roles in regulating carbon flux networks. Further bioinformatics analysis highlighted the potential links between these genes and central metabolic pathways, offering new targets for metabolic engineering. Additionally, alterations in transcription factors associated with carbon flux regulation were identified, suggesting the existence of previously unexplored regulatory mechanisms. These observations not only provide deeper insights into the regulatory network of central carbon metabolism in *E. coli*, but also offer novel perspectives for systems biology research and metabolic engineering applications.

Differential gene expression was analyzed through KEGG functional enrichment to investigate the metabolic pathways involved in cytidine synthesis at 39 h of fermentation (Fig. 4). The resulting map of DEGs highlights the involvement of key genes in the glycolytic pathway. In  $K12\Delta poxB$ , all genes related to glycolysis were upregulated to varying degrees compared to the K12 strain, indicating that the knockout of *poxB* impacts the entire glycolysis pathway. Specifically, the *acs* gene was activated, helping to maintain the cellular acetic acid metabolic state. In contrast, in the  $K12\Delta poxB\Delta pta$  strain, the *pgi* gene was significantly downregulated relative to the K12 strain, suggesting that changes in acetic acid metabolism may affect the activity of glucose-6-phosphate isomerase, potentially hindering the conversion of glucose to glucose-6-phosphate and conserving carbon sources [32]. PRPP, a critical precursor in cytidine synthesis [33], was found to be upregulated in the *poxB* and *pta* knockout strains, thereby enhancing cytidine production. However, no significant differences in gene expression were observed for other glycolytic enzymes between  $K12\Delta poxB\Delta pta$  and  $K12\Delta poxB$ , indicating that *pta* deletion does not alter alternative glycolytic pathways. Energy metabolism pathways linked to glycolysis in  $K12\Delta poxB\Delta pta$  remained unchanged, with carbon flux redirected toward cytidine synthesis pathways, while glycolytic energy production remained constant. These results align with the findings of Liu et al. [19] and the residual sugar measurements reported previously, further confirming the enhanced cytidine production. Additionally, the majority of glycolysis-related genes were downregulated in  $K12\Delta poxB\Delta pta$  relative to  $K12\Delta poxB$ , with the most notable downregulation observed in the *pgi* and *acs* genes. These results suggest that the deletion of *pta* compromises the functionality of glucose-6-phosphate isomerase and reduces acetic acid production, thereby stabilizing the cellular environment and redirecting carbon flux

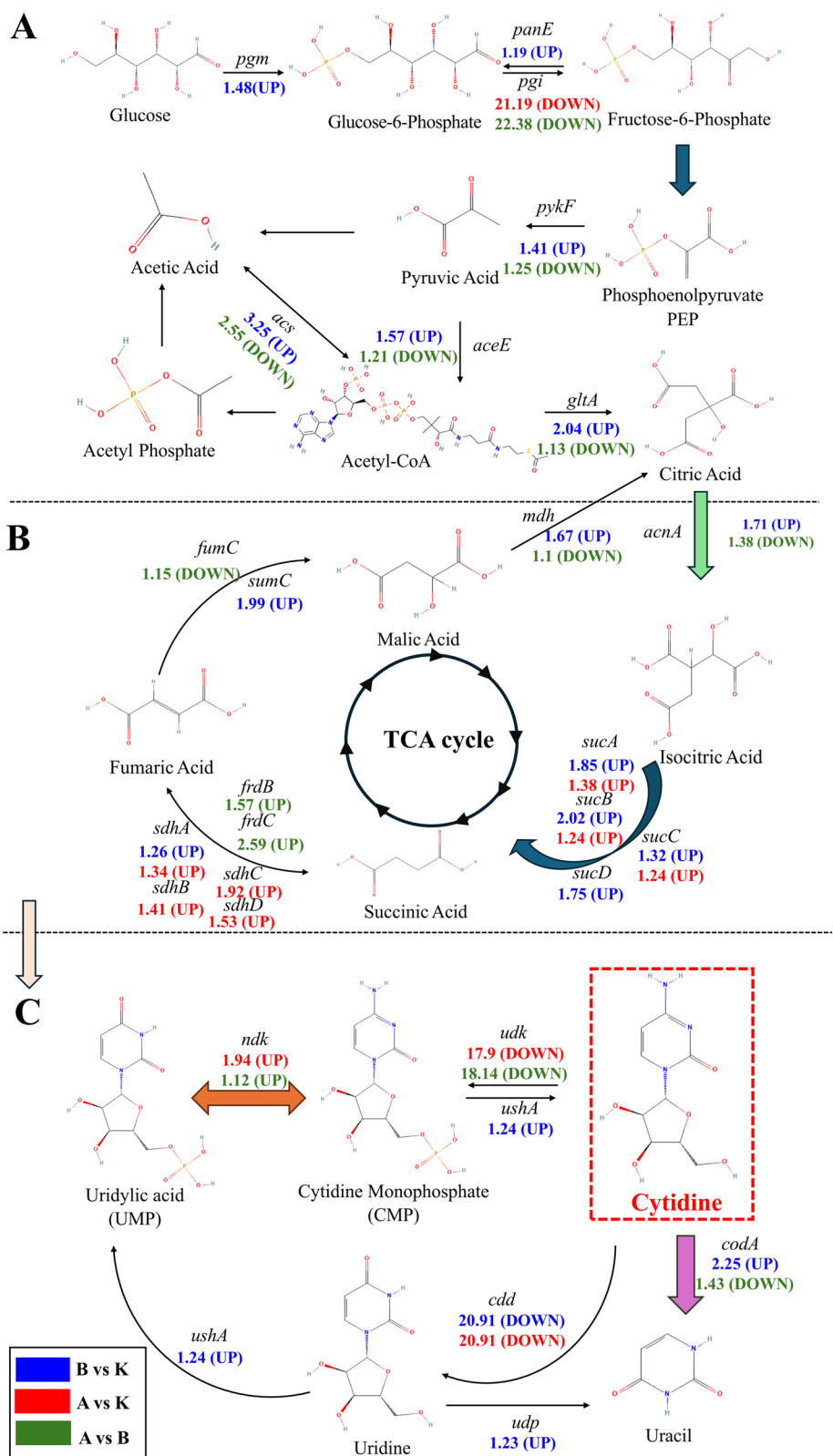


**Fig. 4** Pathway map of differentially expressed genes involved in cytidine synthesis across the comparison groups: **A** glycolytic pathway; **B** TCA cycle; **C** cytidine synthesis pathways. Each pathway is colour-coded to reflect the corresponding comparison groups. In the figure, K denotes strain K12, B denotes strain K12Δ*poxB*, and A denotes strain K12Δ*poxB*Δ*pta*. “UP” indicates upregulation of gene expression, and “DOWN” indicates downregulation of gene expression

towards cytidine biosynthesis. These observations are consistent with the pH assay and cytidine measurement results discussed earlier. In the TCA cycle, most genes associated with this pathway were upregulated in K12 $\Delta$ *poxB* compared to K12. This suggests that *poxB* knockout enhances cytidine production by modulating energy metabolism and substrate synthesis. This is consistent with our earlier findings indicating that increased ATP production during glycolysis plays a significant role in boosting cytidine synthesis. Further comparison between K12 $\Delta$ *poxB* $\Delta$ *pta* and K12 revealed upregulation of the *sucABC* and *sdhABCD* genes involved in the succinate synthesis pathway, suggesting that the double knockout of *poxB* and *pta* genes disrupts the TCA cycle, thereby affecting succinate production. As a result, cofactors such as NADH and ATP are produced in higher quantities, which in turn promotes an increase in cytidine production. These findings are consistent with our previous results (Fig. 3D). When comparing K12 $\Delta$ *poxB* $\Delta$ *pta* to K12 $\Delta$ *poxB*, the upregulation of the *frdBC* gene, associated with fumarate synthesis, was observed. This gene regulates the conversion of fumarate to succinate, implying a potential increase in succinate—a key substrate for cytidine biosynthesis. Furthermore, the downregulation of the *fumC* gene indicates a corresponding reduction in malate, which is known to be cytotoxic. This is consistent with earlier observations from the growth curve (Fig. 3B) [34]. Taken together, these results suggest that the knockout of acetate metabolism genes in *E. coli* may not only promote cytidine biosynthesis but also enhance cellular environment stability. In the context of cytidine biosynthesis, K12 $\Delta$ *poxB* displayed downregulation of several key genes, particularly the *cdd* gene, which encodes cytidine/deoxycytidine deaminase. This resulted in a reduced conversion of cytidine into its metabolic byproduct, uracil. These results suggest that the knockout of the *poxB* gene may increase cytidine production by disrupting the uracil synthesis pathway. However, the increase in cytidine production was not substantial, likely due to the activation of the uracil production pathway, which consequently depletes cytosine. This suggests a compensatory mechanism whereby the activation of uracil biosynthesis consumes cytosine, limiting the increase in cytidine production. To maintain pyrimidine and nucleoside homeostasis, the cell compensates by enhancing the consumption and metabolism of cytidine. A comparison of K12 and K12 $\Delta$ *poxB* $\Delta$ *pta* also revealed significant downregulation of the *udk* gene, which is responsible for the catabolism of cytidine to cytidine monophosphate. In contrast, the *ndk* gene, which catalyzes the conversion of CTP to CDP and UDP to UTP, was significantly upregulated.

These results suggest that the *pta* gene knockout in *E. coli* facilitates an increase in cytidine production by reducing the reverse reaction of cytidine metabolism. This reduction in reverse isomerization enhances the flow of carbon metabolism toward cytidine synthesis, further supporting the hypothesis that *pta* deletion promotes cytidine production. The alteration of the cellular pH environment may contribute to this change, consistent with previous research [35]. Comparison of K12 $\Delta$ *poxB* $\Delta$ *pta* with K12 $\Delta$ *poxB* revealed, in addition to changes in the *udk* and *ndk* genes, a downregulation of *codA*, which mediates the conversion of cytosine to uracil. These results suggest that pyrimidine metabolism in the cells reached equilibrium, corroborating our previous findings (Fig. 3D). RT-qPCR validation of the DEGs (*gltA*, *pgi*, *udk*, *cdd*, and *acs*) shown in Fig. S13 demonstrated that the expression trends and statistical significance were consistent with transcriptomic data, supporting the reliability of the transcriptomic analysis. In summary, knockout of the *poxB* gene likely altered the energy metabolism of *E. coli*, while the double knockout of *poxB* and *pta* may have shifted the carbon metabolic flux, promoting cytidine production. The transcriptomic data could provide a foundation for subsequent investigations aimed at optimizing carbon and energy fluxes through targeted modification of the tricarboxylic acid cycle pathway in *E. coli*. This strategy requires a comprehensive understanding and precise regulation of metabolic pathways, particularly the key enzymes and regulators involved in cytidine biosynthesis. Furthermore, identifying genes such as *sucABCD*, *pyrB*, *fumABC*, and *acnABC*, which are critical for cytidine synthesis, is essential for enhancing cytidine production efficiency through metabolic engineering. This process involves not only improving precursor supply and intermediate conversion efficiency but also addressing bottlenecks in the metabolic pathways, along with optimizing cytidine transport and accumulation [36]. However, the underlying mechanisms driving the observed effects on cytidine synthesis require further investigation.

#### Metabolomic analysis reveals distinct metabolic control of *poxB* and *pta* deletion in *E. coli*

To explore the causes and mechanisms underlying the changes in cytidine production in *E. coli* following knockout of the *poxB* and *pta* genes, metabolomics was employed to identify differentially abundant metabolites at the conclusion of fermentation (39 h). Analysis revealed that the metabolomic data were highly predictive, providing valuable insights for subsequent trials (see Figs. S14–S18 for metabolomics quality control results). Fig. S19 illustrates the classification of differentially abundant

metabolites and KEGG functional enrichment across various comparison groups. The differentially abundant metabolites primarily include carboxylic acids and their derivatives, fatty acids, organic oxides, pyrimidine nucleosides, quinolines, and their derived steroids (Fig. S19A, B). These metabolites are essential for regulating intracellular pH, controlling energy metabolism, and facilitating cellular signaling. They also play a significant role in maintaining the balance between redox and carbon metabolism, synthesizing pyrimidine nucleosides, and modulating membrane transport functions in *E. coli* cells. These results suggest that the knockout of the acetate metabolism genes *poxB* and *pta* primarily disrupts acetate metabolism, nucleoside metabolism, and carbon metabolic flux in *E. coli*, consistent with the conclusions of our previous studies (Fig. S9C).

To further elucidate the primary biological functions of the differentially abundant metabolites, KEGG functional enrichment analysis was performed across several categories, including cellular processes, environmental information processing, genetic information processing, and metabolism. This analysis aimed to investigate the functions and roles of the differentially abundant metabolites across distinct comparison groups (Fig. S20). The KEGG functional enrichment map of these metabolites revealed predominant enrichment in the categories of cellular environmental information processing and metabolism. Notably, the key differentially abundant metabolites involved in environmental information processing were primarily associated with the ABC transporter system, which governs membrane transport. This suggests that knockout of the *poxB* and *pta* genes in *E. coli* may enhance cytidine production by altering cell membrane permeability and modulating intracellular energy metabolism. Increased membrane permeability facilitates the transfer of metabolites, thereby boosting cytidine production [37], a finding that aligns with a previous study (Fig. 3B, C; Fig. S9C). Furthermore, Fig. S20 highlights a significant number of differentially abundant metabolites associated with *E. coli* metabolism, indicating that disruption of key acetate metabolism genes can substantially alter the metabolic processes of *E. coli*. Compared to the K12 strain, the differentially abundant metabolites in the K12 $\Delta$ *poxB* strain were primarily associated with amino acid metabolism (n=20), nucleotide metabolism (n=17), pyrimidine metabolism (n=9), carbon metabolism (n=7), and the tricarboxylic acid cycle (n=3). These results suggest that *poxB* gene knockout enhances cytidine production by modulating amino acid synthesis, nucleotide formation, and carbon metabolic flux in *E. coli*. In contrast, the differentially abundant metabolites in K12 $\Delta$ *poxB* $\Delta$ *pta* were predominantly linked to amino

acid metabolism (n=17), nucleotide metabolism (n=9), pyrimidine metabolism (n=6), and cofactor biosynthesis (n=13). This suggests that the combined knockout of both *poxB* and *pta* genes may reduce intracellular acetate metabolism, while enhancing energy flow and carbon metabolism, thus promoting cytidine production. Compared to K12 $\Delta$ *poxB*, the differentially abundant metabolites in K12 $\Delta$ *poxB* $\Delta$ *pta* were notably enriched in amino acid metabolism (n=10), nucleotide metabolism (n=8), pyrimidine metabolism (n=5), carbon metabolism (n=6), and the TCA cycle (n=3). This further corroborates the notion that *pta* gene knockout facilitates a more efficient redirection of cellular carbon flux toward cytidine synthesis. Metabolomic analysis also revealed that in the *poxB* and *pta* double knockout strains, *E. coli* activates the corresponding acid backfill pathways. These pathways are typically induced under acidic stress to neutralize accumulated acids and protect the cell from damage. In the *poxB* and *pta* knockout strains, these pathways lead to increased synthesis of acidic amino acids (e.g., aspartate and glutamate) and nucleotides (e.g., phosphorylated adenosine and guanosine). The accumulation of these metabolites lowers the pH of the culture medium, thus creating a more favorable environment for bacterial growth [21, 38, 39]. These results are consistent with prior transcriptomic studies and provide additional insight into how disruption of key genes involved in acetic acid metabolism can enhance cytidine production by modulating carbon flux and intracellular energy dynamics. However, the precise mechanisms underlying these effects and their interactions require further investigation.

To examine the metabolic diversity before and after gene knockout, a heatmap of differentially abundant metabolites was constructed to highlight the principal metabolites affected. As shown in Fig. S21A, compared to the K12 strain, the metabolites significantly elevated in K12 $\Delta$ *poxB* were primarily amino acids and their derivatives, nucleosides and nucleotide derivatives, along with a few alkaloids. Amino acids and their derivatives are involved in regulating nitrogen metabolism and maintaining cellular stability. The heatmap illustrates an increase in the synthesis of glutamate-related amino acid derivatives or dipeptides, suggesting enhanced activity in the glutamate biosynthesis pathway in K12 $\Delta$ *poxB*. This may be a key factor driving the increased cytidine production in this strain. Additionally, cytidine itself is a markedly upregulated metabolite, consistent with the previous cytidine measurements. On the other hand, the significantly downregulated metabolites in this comparison were predominantly amino acids and their derivatives. These results suggest that the *poxB*

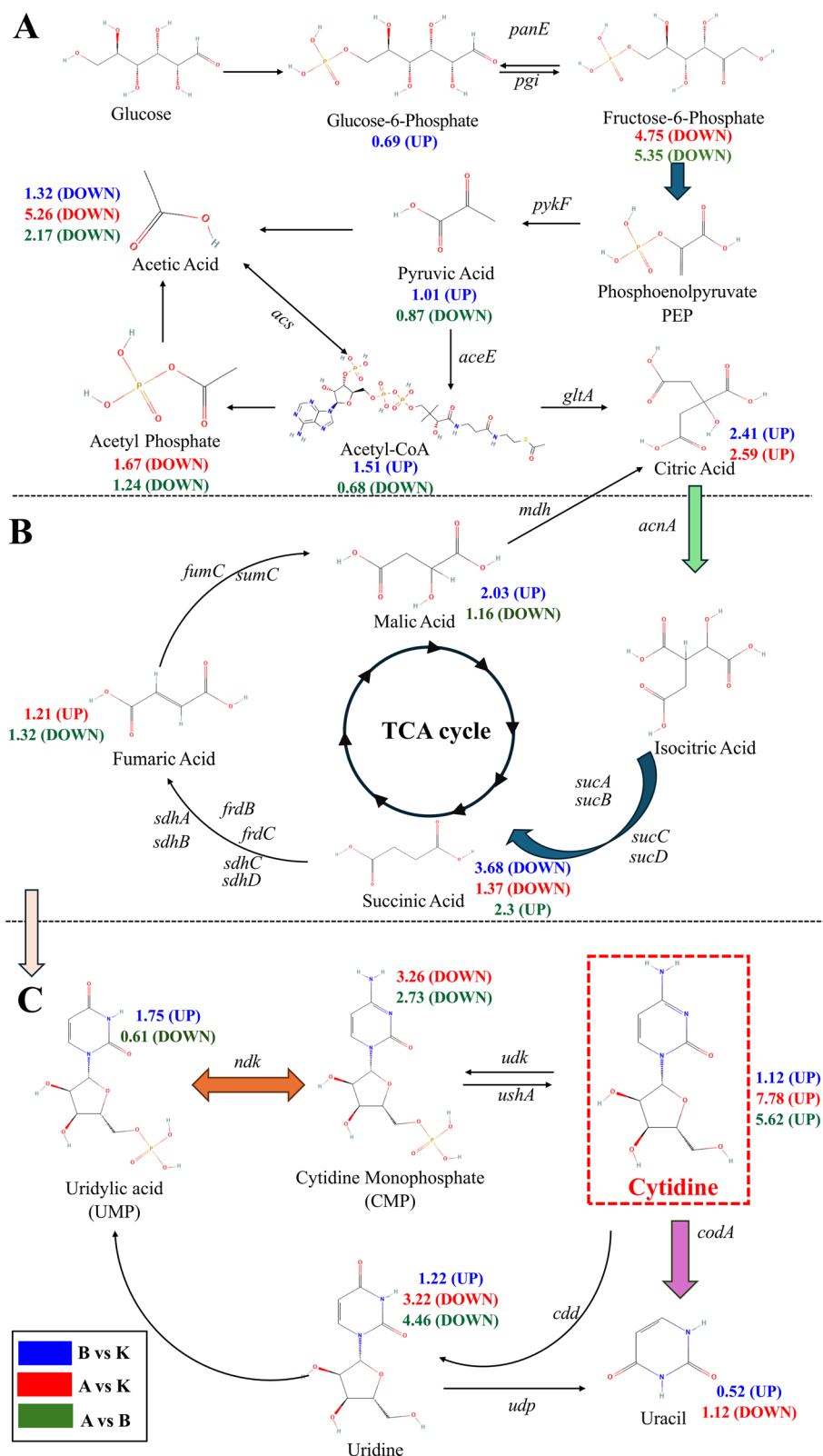
gene knockout in *E. coli* induces a reorganization of both carbon and nitrogen fluxes, effectively redirecting metabolic pathways to support cytidine biosynthesis. In the K12 $\Delta$ *poxB* $\Delta$ *pta* strain, as shown in Fig. S21B, cytidine was again identified as a prominently upregulated metabolite, confirming the earlier cytidine measurement data. The downregulated metabolites primarily consisted of organic acids, including acetic acid, suggesting that the reduced flux through organic acid metabolism may contribute to the slower pH decline and the increase in bacterial growth observed in Fig. 3A, B. Additionally, the downregulation of other amino acid metabolites further supports the notion that both carbon and nitrogen sources are redirected toward cytidine production. This redirection likely plays a significant role in the enhanced cytidine synthesis observed following the knockout of both *poxB* and *pta* (Fig. S22). In summary, the sequential knockout of the critical *poxB* and *pta* genes in *E. coli*'s acetic acid metabolism can substantially boost cytidine production by limiting the accumulation of byproducts like acetic acid. Further investigation is required to pinpoint the specific metabolic pathway alterations responsible for this effect.

Figure 5 illustrates the differentially abundant metabolites in the cytidine synthesis pathway across strains K12, K12 $\Delta$ *poxB*, and K12 $\Delta$ *poxB* $\Delta$ *pta*, with the multiplicity of differences in the metabolites indicated alongside the respective compounds. Compared to the K12 strain, the principal upregulated metabolites in K12 $\Delta$ *poxB* were 2-phosphoglycerate, pyruvate, and acetyl-CoA, all of which play critical roles in energy metabolism and carbon cycling. The major downregulated metabolite was acetic acid, indicating that the *poxB* gene knockout enhances glycolytic capacity and enriches the pool of energy and organic carbon, a result consistent with previous research [39]. In K12 $\Delta$ *poxB* $\Delta$ *pta*, metabolism of fructose-6-phosphate, acetyl phosphate, and acetic acid decreased markedly, whereas the metabolism of triose phosphate significantly increased. These alterations suggest an enhancement in ATP and cofactor synthesis in this strain. The observed increase in cytidine production is linked not only to the reduction in acetic acid production but also to the elevation in cofactor levels and other key metabolites (Fig. S9C). When comparing K12 $\Delta$ *poxB* and K12 $\Delta$ *poxB* $\Delta$ *pta*, the downregulated metabolites in K12 $\Delta$ *poxB* $\Delta$ *pta* were primarily acetic acid and acetyl phosphate. Pyruvate and acetyl-CoA were also downregulated, though not significantly different from the K12 strain, likely due to the upregulation of corresponding metabolites in K12 $\Delta$ *poxB*. This aligns with previous transcriptomic and pH measurement data. In the TCA cycle, the synthesis of citric and malic acids

was higher in K12 $\Delta$ *poxB* compared to K12, suggesting that the enhanced energy synthesis in this strain may be a key factor driving increased cytidine production. Additionally, the elevated fumaric acid content and reduced succinic acid content in K12 $\Delta$ *poxB* $\Delta$ *pta* relative to K12 indicate that the *pta* knockout increases both intracellular energy and carbon flux in *E. coli*, further supporting our earlier results. Based on these findings, the synthesis substrate for cytidine, succinic acid, was found to be elevated in K12 $\Delta$ *poxB* $\Delta$ *pta* compared to K12 $\Delta$ *poxB*, corroborating previous transcriptomic and cytidine measurement data. This confirms that *poxB* gene knockout enhances cytidine production by improving precursor synthesis and optimizing carbon source utilization within the cellular environment (Fig. 3C). However, corresponding increases in the levels of uridine and uracil, metabolic byproducts, were also observed, suggesting activation of the cytidine conversion pathway to maintain cellular nucleoside and nitrogen metabolic homeostasis. This activation likely stems from alterations in cell membrane permeability. In comparison with K12, K12 $\Delta$ *poxB* $\Delta$ *pta* exhibited a significant 7.78-fold increase in cytidine levels, coupled with a decrease in CMP and uridine, indicating inhibition of the reverse reaction in cytidine synthesis. Moreover, the deamination of cytidine, which requires acidic conditions, contributed to a marked reduction in uridine production. As a result, side reactions in cytidine biosynthesis in *E. coli* were minimized, leading to enhanced cytidine accumulation. In contrast to K12 $\Delta$ *poxB*, K12 $\Delta$ *poxB* $\Delta$ *pta* showed a pronounced upregulation of cytidine and a significant downregulation of CMP and uridine, suggesting that modifications in carbon metabolic flux due to the *poxB* and *pta* knockouts promote the biosynthetic yield of cytidine. In conclusion, the classification and enrichment of differentially abundant metabolites demonstrated that the knockout of *poxB* and *pta* genes in *E. coli* significantly enhances cytidine synthesis, which is linked to the redirection of carbon metabolism toward cytidine biosynthesis.

## Conclusion

This study investigates the sequential knockout of the *poxB* and *pta* genes in *E. coli*, both critical to acetic acid metabolism, revealing a significantly slower decrease in pH, a substantial reduction in acetic acid production, and a notable increase in cytidine synthesis. Transcriptomic and metabolomic analyses demonstrated that these alterations are linked to changes in intracellular pH and a reorganization of carbon flux within the cell. These findings underscore the pivotal role of acetic acid metabolism in regulating cytidine biosynthesis in *E. coli*,



**Fig. 5** Pathway diagrams of differential metabolites related to the cytidine synthesis pathway in the comparison groups: **A** glycolytic pathway; **B** TCA cycle; **C** cytidine synthesis pathways. Each pathway is colour-coded to reflect the corresponding comparison groups. In the figure, K denotes strain K12, B denotes strain K12Δ*poxB*, and A denotes strain K12Δ*poxB*Δ*pta*. “UP” indicates upregulation of metabolite levels, and “DOWN” indicates downregulation of metabolite levels

providing novel insights and strategies for optimizing *E. coli* as a cell factory for cytidine production. However, several limitations exist in this study, particularly in the application of computational biology. Theoretical yield calculations for cytidine synthesis were not accurately determined, and the functional role of the *pta* gene was not thoroughly dissected through a single knockout experiment, leaving its specific impact on cytidine production unresolved. Future studies may focus on further modifying the amino acid and nucleotide metabolic pathways in *E. coli*, aiming to completely dismantle the acid-suppressed metabolic pathways and thereby enhance cytidine production.

#### Abbreviations

<i>E. coli</i>	<i>Escherichia coli</i>
K12 and K	<i>Escherichia coli</i> K12
K12Δ <i>pxxB</i> and B	<i>Escherichia coli</i> K12Δ <i>pxxB</i>
K12Δ <i>pxxB</i> Δ <i>pta</i> and A	<i>Escherichia coli</i> K12Δ <i>pxxB</i> Δ <i>pta</i>
PCR	Polymerase chain reaction
TCA cycle	Tricarboxylic acid cycle
RT-qPCR	Real-time quantitative PCR
DEGs	Differentially Expressed Genes
VIP	Variables on predicted
PCA	Principal component analysis
PLS-DA	Partial least squares discriminant analysis
OPLS-DA	Orthogonal partial least squares discriminant analysis

#### Supplementary Information

The online version contains supplementary material available at <https://doi.org/10.1186/s12934-025-02657-5>.

Supplementary Material 1.

#### Acknowledgements

We thank Sangon Biotech Shanghai Co., Ltd. for technological assistance in transcriptomics experiment. And we thank Shanghai Bioprofile Technology Company Ltd. for technological assistance in untargeted metabolomics experiment. We would also like to thank EditChecks (<https://editchecks.com.cn/>) for providing linguistic assistance during the preparation of this manuscript.

#### Author contributions

T.Y.: conceptualization, methodology, investigation, software, formal analysis, data curation, resources, writing—original draft; W. D.: methodology, investigation, software, data curation, formal analysis, writing—review & editing; Z. A.: methodology, software, investigation, data curation, formal analysis, visualization; H. Z.: software, data curation, formal analysis; X. W.: investigation, data curation, visualization. J. X.: investigation, data curation; H. L.: resources, visualization, project administration, formal analysis, funding acquisition, writing—review & editing; H. F.: conceptualization, methodology, writing—review & editing, visualization, supervision, project administration, funding acquisition.

#### Funding

This work was supported by Natural Science Foundation of Ningxia, China (grant number 2023AAC02030); the National Natural Science Foundation of China (grant number 31860020); the Ningxia Hui Autonomous Region Youth Top Talent Training Project (grant number 022004000010); the Helanshan Scholars Program of Ningxia University (grant number No. 2020).

#### Availability of data materials

No datasets were generated or analysed during the current study.

#### Declarations

##### Competing interests

The authors declare no competing interests.

##### Author details

<sup>1</sup>School of Life Sciences, Ningxia University, Yinchuan 750021, Ningxia, China. <sup>2</sup>School of Food Science and Engineering, Ningxia University, Yinchuan 750021, Ningxia, China. <sup>3</sup>Ningxia Key Laboratory for Food Microbial-Applications Technology and Safety Control, Ningxia University, Yinchuan 750021, Ningxia, China.

Received: 2 October 2024 Accepted: 18 January 2025

Published online: 04 February 2025

#### References

- Pinhal S, Ropers D, Geiselmann J, de Jong H. Acetate metabolism and the inhibition of bacterial growth by acetate. *J Bacteriol.* 2019;201:e00147–e219.
- Valgepea K, Adamberg K, Vilu R. Decrease of energy spilling in *Escherichia coli* continuous cultures with rising specific growth rate and carbon wasting. *BMC syst biol.* 2011;5:106.
- Renilla S, Bernal V, Fuhrer T, Castaño-Cerezo S, Pastor JM, Iborra JL, et al. Acetate scavenging activity in *Escherichia coli*: interplay of acetyl-CoA synthetase and the PEP-glyoxylate cycle in chemostat cultures. *Appl Microbiol Biotechnol.* 2012;93:2109–24.
- Trcek J, Mira NP, Jarboe LR. Adaptation and tolerance of bacteria against acetic acid. *Appl Microbiol Biotechnol.* 2015;99:6215–29.
- Wang J, Cheng L-K, Chen N. High-level production of L-threonine by recombinant *Escherichia coli* with combined feeding strategies. *Biotechnol Biotechnol Equip.* 2014;28:495–501.
- Luli GW, Strohl WR. Comparison of growth, acetate production, and acetate inhibition of *Escherichia coli* strains in batch and fed-batch fermentations. *Appl Environ Microbiol.* 1990;56:1004–11.
- Bernal V, Castaño-Cerezo S, Cánovas M. Acetate metabolism regulation in *Escherichia coli*: carbon overflow, pathogenicity, and beyond. *Appl Microbiol Biotechnol.* 2016;100:8985–9001.
- Yang J, Wang Z, Zhu N, Wang B, Chen T, Zhao X. Metabolic engineering of *Escherichia coli* and *in silico* comparing of carboxylation pathways for high succinate productivity under aerobic conditions. *Microbiol Res.* 2014;169:432–40.
- Castaño-Cerezo S, Pastor JM, Renilla S, Bernal V, Iborra JL, Cánovas M. An insight into the role of phosphotransacetylase (*pta*) and the acetate/acetyl-CoA node in *Escherichia coli*. *Microb Cell Fact.* 2009;8:54.
- Skorokhodova AY, Gulevich AY, Debabov VG. Optimization of aerobic synthesis of succinic acid from glucose by recombinant *Escherichia coli* strains through the tricarboxylic acid cycle variant mediated by the action of 2-ketoglutarate decarboxylase. *Appl Biochem Microbiol.* 2023;59:786–92.
- Ravi SN, Sankaranarayanan M. Enhanced synthesis of 3-hydroxypropionic acid by eliminating by-products using recombinant *Escherichia coli* as a whole cell biocatalyst. *Top Catal.* 2024;67:169–80.
- Ghamsari PA, Samadzadeh M, Mirzaei M. Halogenated derivatives of cytidine: structural analysis and binding affinity. *J Theor Comput Chem.* 2020;19:2050033.
- Iglesias LE, Lewkowicz ES, Medici R, Bianchi P, Iribarren AM. Biocatalytic approaches applied to the synthesis of nucleoside prodrugs. *Biotechnol Adv.* 2015;33:412–34.
- Dong H, Liu Y, Zu X, Li N, Li F, Zhang D. An enzymatic assay for high-throughput screening of cytidine-producing microbial strains. *PLoS ONE.* 2015;10: e0121612.
- Han B, Dai Z, Li Z. Computer-based design of a cell factory for high-yield cytidine production. *ACS Synth Biol.* 2022;11:4123–33.
- Dai Z, Han B, Li Z, Li Z. Modularized reconstruction of pyrimidine pathway in *Escherichia coli* for enhanced pyrimidine nucleosides biosynthesis. *Biochem Eng J.* 2023;200: 109101.

17. Yang K, Li Z. Multistep construction of metabolically engineered *Escherichia coli* for enhanced cytidine biosynthesis. *Biochem Eng J*. 2020;154:107433.
18. Kotte O, Volkmer B, Radzikowski JL, Heinemann M. Phenotypic bistability in *Escherichia coli*'s central carbon metabolism. *Mol Syst Biol*. 2014;10:736.
19. Liu F, Ye T, Zhang X, Ma C, Liu H, Fang H. The effect of *E. coli* uridine-cytidine kinase gene deletion on cytidine synthesis and transcriptome analysis. *Fermentation*. 2022;8:586.
20. Gece G, Labunskaitė R, Pedersen M, Kilstrop M, Johanson T. Minimizing acetate formation from overflow metabolism in *Escherichia coli*: comparison of genetic engineering strategies to improve robustness toward sugar gradients in large-scale fermentation processes. *Front Bioeng Biotechnol*. 2024;12:1339054.
21. Enjalbert B, Millard P, Dinclaux M, Portais J-C, Létisse F. Acetate fluxes in *Escherichia coli* are determined by the thermodynamic control of the Pta-AckA pathway. *Sci Rep*. 2017;7:42135.
22. Zhang S, Yang W, Chen H, Liu B, Lin B, Tao Y. Metabolic engineering for efficient supply of acetyl-CoA from different carbon sources in *Escherichia coli*. *Microb Cell Fact*. 2019;18:130.
23. Zhang X, Liu L, Ma C, Zhang H, Liu H, Fang H. Improving the level of the cytidine biosynthesis in *E. coli* through atmospheric room temperature plasma mutagenesis and metabolic engineering. *J Appl Microbiol*. 2024;135:133.
24. Fang H, Xie X, Xu Q, Zhang C, Chen N. Enhancement of cytidine production by coexpression of *gnd*, *zwf*, and *prs* genes in recombinant *Escherichia coli* CYT15. *Biotechnol Lett*. 2013;35:245–51.
25. Li Z, Nees M, Bettenbrock K, Rinas U. Is energy excess the initial trigger of carbon overflow metabolism? Transcriptional network response of carbon-limited *Escherichia coli* to transient carbon excess. *Microb Cell Fact*. 2022;21:67.
26. Li M, Yao S, Shimizu K. Effect of *poxB* gene knockout on metabolism in *Escherichia coli* based on growth characteristics and enzyme activities. *World J Microbiol Biotechnol*. 2007;23:573–80.
27. Skorokhodova AY, Gulevich AY, Debabov VG. Engineering *Escherichia coli* for respiro-fermentative production of pyruvate from glucose under anoxic conditions. *J Biotechnol*. 2019;293:47–55.
28. Wang T, Shen P, He Y, Zhang Y, Liu J. Spatial transcriptome uncovers rich coordination of metabolism in *E. coli* K12 biofilm. *Nat Chem Biol*. 2023;19:940–50.
29. Wong GT, Bonocora RP, Schep AN, Beeler SM, Lee Fong AJ, Shull LM, et al. Genome-wide transcriptional response to varying RpoS levels in *Escherichia coli* K-12. *J Bacteriol*. 2017. <https://doi.org/10.1128/jb.00755-16>.
30. Hayes ET, Wilks JC, Sanfilippo P, Yohannes E, Tate DP, Jones BD, et al. Oxygen limitation modulates pH regulation of catabolism and hydrogenases, multidrug transporters, and envelope composition in *Escherichia coli* K-12. *BMC Microbiol*. 2006;6:89.
31. Dittrich CR, Vadali RV, Bennett GN, San K-Y. Redistribution of metabolic fluxes in the central aerobic metabolic pathway of *E. coli* mutant strains with deletion of the *ackA-pta* and *poxB* pathways for the synthesis of isoamyl acetate. *Biotechnol Progr*. 2005;21:627–31.
32. Hollinshead WD, Rodriguez S, Martin HG, Wang G, Baidoo EEK, Sale KL, et al. Examining *Escherichia coli* glycolytic pathways, catabolite repression, and metabolite channeling using  $\delta$ pfk mutants. *Biotechnol Biofuels*. 2016;9:212.
33. Zhang K, Qin M, Hou Y, Zhang W, Wang Z, Wang H. Efficient production of guanosine in *Escherichia coli* by combinatorial metabolic engineering. *Microb Cell Fact*. 2024;23:182.
34. Guo F, Wu M, Dai Z, Zhang S, Zhang W, Dong W, et al. Current advances on biological production of fumaric acid. *Biochem Eng J*. 2020;153:107397.
35. Maurer LM, Yohannes E, Bondurant SS, Radmacher M, Slonczewski JL. pH regulates genes for flagellar motility, catabolism, and oxidative stress in *Escherichia coli* K-12. *J Bacteriol*. 2005;187:304–19.
36. Park SY, Eun H, Lee MH, Lee SY. Metabolic engineering of *Escherichia coli* with electron channelling for the production of natural products. *Nat Catal*. 2022;5:726–37.
37. Rees DC, Johnson E, Lewinson O. ABC transporters: the power to change. *Nat Rev Mol Cell Biol*. 2009;10:218–27.
38. Gatsios A, Kim CS, Crawford JM. *Escherichia coli* small molecule metabolism at the host–microorganism interface. *Nat Chem Biol*. 2021;17:1016–26.
39. Phue J-N, Lee SJ, Kaufman JB, Negrete A, Shiloach J. Acetate accumulation through alternative metabolic pathways in *ackA* (-) *pta* (-) *poxB* (-) triple mutant in *E. coli* B (BL21). *Biotechnol Lett*. 2010;32:1897–903.

## Publisher's Note

Springer Nature remains neutral with regard to jurisdictional claims in published maps and institutional affiliations.